Control of the atmospheric flight phase of small rocket launchers

Miguel de Freitas Dias
miguel.f.dias@ist.utl.pt

Instituto Superior Técnico, Universidade de Lisboa, Portugal
April 2017

***Abstract*—This paper addresses Thrust Vectoring Control (TVC) design techniques for small launch vehicles with bounded roll-rate. The first contribution is a 6 DoF nonlinear model that serves as a tool for flight control system design. The nonlinear model is then trimmed and linearized, yielding a set of linear models. Building upon this result, a decoupled lateral and longitudinal PID controller is designed, as well as a LQR controller. Using the full nonlinear model a backstepping controller is developed. Particular emphasis is given to the analysis of the resulting closed-loop system under the presence of different disturbances that can affect the system using Lyapunov stability analysis. From the robustness analysis of the nonlinear controller it arises that specific inaccuracies in the position of the center of mass can be corrected, thus an adaptive backstepping controller is developed to account for this. Finally, a comparison between the performance of the designed linear and nonlinear controllers is carried out and a discussion about the adaptability of the designed controller to other launch vehicles is presented.**

***Index Terms*—6 DoF modelling, Launch Vehicle, LQR, PID, Backstepping, Lyapunov Design**

I. Introduction

RECENT studies show that there has been an increase in the total number of spacecraft launched into space over the past ten years, with potential growth over the next decade [1]. Small satellites have attracted the interest of scientific research entities and private commercial enterprises alike [2].

Small satellites are usually launched as secondary payload on a larger mission, which has obvious limitations in terms of the launch date and final orbit for the satellite, as the mission is developed for the primary cargo. Thus, there have been efforts to develop smaller launch vehicles (LVs), designed to take light payloads to LEO. Regarding LVs, there are several options with different design parameters and mission requirements, manufactured both by government agencies or private companies. Evidently, all these different launch systems need control algorithms to steer its cargo into the final orbit. The starting point of this work is a study of control systems for the atmospheric flight phase of rocket launchers, using linear and nonlinear control techniques.

Usually linear methods are preferred in the design of controllers for this flight phase [3]–[5], due to years of experience and consolidation of the theory, as well as reliable and well documented design procedures. Nonetheless, nonlinear control techniques have also been proposed [6], [7], although nonlinear control is typically used in later stages of the mission.

In line with these trends, the objective of this work can be summarised as follows:

- Formulate a dynamical model of a generic rocket launch vehicle, with symmetric geometry and flexible modes;
- Follow the classical linear control design process for the modelled vehicle;
- Design of a nonlinear controller for the vehicle;
- Compare the performance of the designed controllers;
- Evaluate the ability to apply the designed controllers to other rocket launchers with minimum effort.

The organization of this paper is as follows. In section II the 6 Degree of Freedom (DoF) model of a generic LV is presented. Section III describes the classical linear control process used for these systems. The core of this work is presented in Section IV, where a nonlinear controller is developed for the LV. Section V presents a comparison between the designed control systems. Finally, some concluding remarks and directions for future work are presented in Section VI.

II. LV modelling

The formulation of the dynamical model for control uses publicly available data related with the VEGA launcher [8]–[16], complemented with data from Deimos Engenharia.

This work focuses on the atmospheric flight phase, before the separation of the first stage, comprising approximately the first 100 seconds of the mission. Control of the first stage is carried out through a TVC system, that allows swivelling of a gimbaled nozzle around a pivot point, with a maximum deflection of $\pm 6.5°$. The TVC system allows control of the pitch and yaw attitude, while the roll-rate is limited by four of the six Roll and Attitude Control System (RACS) thrusters [8]. The roll attitude is limited if it exceeds the threshold $|p| > 45°/s$ [11], but is not actively controlled by the TVC system. The choice of this threshold is not arbitrary since the pitch and yaw dynamics are coupled in the presence of roll [9], as will become evident further ahead in this Section. The designed controllers need to be robust to bounded roll-rates under the defined threshold.

Another important definition for the control design is that of the reference trajectory, as it affects the controller synthesis. There are multiple possibilities of defining the trajectory, such as ECI coordinates, Euler angles or quaternions, and the latter are the two most used.

Describing the problem in terms of quaternions eliminates the known issues with Euler angles singularities [17]. However, using appropriate definitions of reference frames makes it possible to guarantee that the reference trajectory lies far from the singularities. Euler angles provide a direct physical interpretation of the position of the vehicle, while the quaternion description does not lend itself to a simple visualisation of the attitude of the vehicle. Therefore, it is chosen to use Euler angles to define the reference trajectory. The controller synthesis described in this dissertation (both linear and nonlinear) using Euler angles could be developed using quaternions as well, with different variables and yielding a different control law, but with similar closed-loop performance. For a description of rigid bodies attitude dynamics using quaternions, the interested reader is refered to [18], [19].

LVs are essentially long slender beams, hence are structurally flexible. The IMU is not located at the center of mass of the vehicle,

therefore it measures the rigid body motion as well as local elastic distortions caused by structural flexibility. These measurements will be fed to the TVC system, which can excite the structural flexible modes and lead to instability. When considering linear control, the first flexible mode frequency is usually close to the crossover regime of the controller, hence the control system has the potencial to excite the flexible modes and destabilize the system [20]. Thus it is important to model the flexible modes of the LV. Now that the important phenomena affecting a LV are defined, the derivation of a general dynamic model is detailed.

Definition of reference frames

Several reference frames are necessary to define the complete set of equations of motion. Figure 1 shows the relation between the ECI reference frame, and the launch point reference frame.

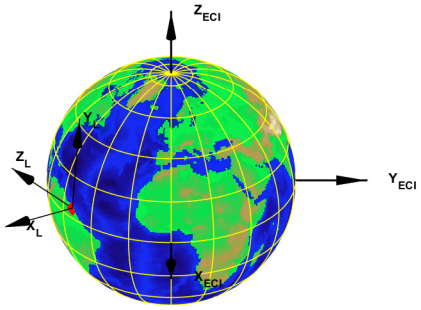

Fig. 1: ECI and launch site reference frames

For simplicity, the Inertial Planetocentric (IP) reference frame will be considered as the inertial reference frame. The difference between the ECI and the IP reference frames is that in the latter the x-axis is defined by the zero-longitude meridian at zero time (time of the launch) [21], hence only two parameters are needed to describe the location of a point relative to the surface of the Earth.

The launch point reference frame (also shown in Figure 1) is characterized as follows: the y_L-z_L plane is tangent to the surface of the Earth at the launch point, with y_L pointing towards the north and z_L pointing towards west. The x_L-axis is perpendicular to the y_L and z_L axes and points towards the sky.

A body-fixed reference frame is also defined for the derivation of the equations of motion. The origin of the body-fixed reference frame is the center of mass of the launcher, with the x_B-axis aligned along the longitudinal axis of the spacecraft. The body fixed reference frame is aligned with the launch reference frame at the time of the launch.

The launch site is the European Spaceport, located at Kourou, in the French Guiana. Its coordinates are δ = 5º 12' 03" N, τ = 52º 45' 59" W (respectively for latitude and longitude) [8].

The rotation matrix from the the body frame to the inertial frame can be obtained as the multiplication of two rotations: the rotation from the launch point to the body reference frame ans the rotation from the launch point to the inertial reference frame, i.e. ${}^B_I\mathbf{R} = {}^B_L\mathbf{R}\,{}^L_I\mathbf{R}$. The first rotation is defined by Euler angles and is expressed in (1), [18], [22].

$$ {}^B_L\mathbf{R} = \begin{bmatrix} c\theta c\psi & c\theta s\psi & -s\theta \\ s\phi s\theta c\psi - c\phi s\psi & s\phi s\theta s\psi + c\phi c\psi & s\phi c\theta \\ c\phi s\theta c\psi + s\phi s\psi & c\phi s\theta s\psi - s\phi c\psi & c\phi c\theta \end{bmatrix}. \quad (1) $$

Since the reference trajectory is defined using Euler angles, it is important to know their dynamics. The set of Euler angles is denoted by $\boldsymbol{\lambda}$ and its derivative, $\dot{\boldsymbol{\lambda}}$, is of the form $\dot{\boldsymbol{\lambda}} = f(\phi,\theta)\,{}^B\boldsymbol{\omega}_B$. The expression for these derivatives are readily available in the literature ([17], [18] or [21]):

$$ \dot{\boldsymbol{\lambda}} = \begin{cases} \dot{\phi} = p + \sin\phi\tan\theta\cdot q + \cos\phi\tan\theta\cdot r \\ \dot{\theta} = \cos\phi\cdot q - \sin\phi\cdot r \\ \dot{\psi} = \frac{\sin\phi}{\cos\theta}\cdot q + \frac{\cos\phi}{\cos\theta}\cdot r. \end{cases} \quad (2) $$

The second rotation depends on the Earth's angular velocity, Ω_e, and the location of the launch point: ${}^I_L\mathbf{R} = \mathbf{R}(\delta,\tau)\cdot\mathbf{R}(\Omega_e,t)$, where:

$$ \mathbf{R}(\delta,\tau) = \begin{bmatrix} \cos\delta\cos\tau & \cos\delta\sin\tau & \sin\delta \\ -\sin\delta\cos\tau & -\sin\delta\sin\tau & \cos\delta \\ \sin\tau & \cos\tau & 0 \end{bmatrix}. \quad (3) $$

and

$$ \mathbf{R}(\Omega_e,t) = \begin{bmatrix} \cos\Omega_e t & -\sin\Omega_e t & 0 \\ \sin\Omega_e t & \cos\Omega_e t & 0 \\ 0 & 0 & 1 \end{bmatrix}. \quad (4) $$

External forces acting on the body

The external forces acting on the vehicle are gravity, propulsion and aerodynamic forces (lift and drag). In order to obtain the equations of motion it is necessary to write these forces in the body-fixed reference frame.

The propulsion system can be swivelled around the pivot point in two different directions, generating pitch and yaw moments to control the trajectory. Hence the transformation of the thrust force from the TVC reference frame to body axes needs to be defined. To do so, consider that the thrust vector lies along the x_B-axis. A negative rotation around the y_B-axis is performed, generating a pitching moment. The angle of rotation is δ_p. Next, perform a negative rotation around the z-axis, generating a yaw moment. The angle associated with this second rotation is δ_y. Furthermore, in rocket launchers, it is common to have the TVC system rotated from the principal axis of the vehicle. Therefore, a rotation of $\Delta\alpha = -45°$ around the x_B-axis is applied. The rotation matrix from the body reference to the TVC reference frame is given by the multiplication of the three elementary rotations defined earlier, in the sequence $\mathbf{R}_x(-45°) \leftarrow \mathbf{R}_1(-\delta_p) \leftarrow \mathbf{R}_2(-\delta_y)$:

$$ {}^T_B\mathbf{R} = \begin{bmatrix} c\delta_p c\delta_y & s\delta_y c\delta_p & s\delta_p \\ \frac{\sqrt{2}}{2}(s\delta_y + c\delta_y s\delta_p) & \frac{\sqrt{2}}{2}(s\delta_y s\delta_p - c\delta_y) & -\frac{\sqrt{2}}{2}c\delta_p \\ \frac{\sqrt{2}}{2}(c\delta_y s\delta_p - s\delta_y) & \frac{\sqrt{2}}{2}(s\delta_y s\delta_p + c\delta_y) & -\frac{\sqrt{2}}{2}c\delta_p \end{bmatrix}. \quad (5) $$

With this definition, the thrust expressed in the body frame is given by ${}^B\mathbf{T} = {}^B_T\mathbf{R}\cdot[T\ 0\ 0]^T$.

The aerodynamic forces expressed in the aerodynamic reference frame are ${}^A\mathbf{F}_a = [-D\ L\ 0]$. This frame is related to the body-fixed frame by the two aerodynamic angles: the angle of attack α and the sideslip angle β. This rotation can be found in [21] and is given by:

$$ {}^A_B\mathbf{R} = \begin{bmatrix} \cos\beta\cos\alpha & \sin\beta & \cos\beta\sin\alpha \\ -\sin\beta\cos\alpha & \cos\beta & -\sin\beta\sin\alpha \\ -\sin\alpha & 0 & \cos\alpha \end{bmatrix}. \quad (6) $$

LV equations of motion

With the forces identified in the previous section and the definition of the inertial frame of reference, Newton's second law yields:

$$ m\,{}^L\dot{\mathbf{v}} + \dot{m}\,{}^L\mathbf{v} = {}^L_B\mathbf{R}\left({}^B\mathbf{T} + {}^B\mathbf{F}_A + {}^B\mathbf{F}_g\right). \quad (7) $$

The inertial velocity is defined as ${}^L\mathbf{v} = {}^L_B\mathbf{R}\,{}^B\mathbf{v}$. Differentiating:

$$ \begin{aligned} {}^L\dot{\mathbf{v}} &= {}^L_B\dot{\mathbf{R}}\,{}^B\mathbf{v} + {}^L_B\mathbf{R}\,{}^B\dot{\mathbf{v}} \\ &= {}^L_B\mathbf{R}\left(\mathbf{S}(\boldsymbol{\omega})\,{}^B\mathbf{v} + {}^B\dot{\mathbf{v}}\right), \end{aligned} \quad (8) $$

where $\mathbf{S}(\boldsymbol{\omega})$ is a skew-symmetric matrix and ${}^{B}\mathbf{v} = [u\ v\ w]^T$ represents the linear velocity vector, expressed in the body-fixed reference frame. Joining equations (7) and (8) yields the expression for the linear acceleration in the body axis:

$$ {}^{B}\dot{\mathbf{v}} = \frac{1}{m}\left({}^{B}\mathbf{T} + {}^{B}\mathbf{F}_A + {}^{B}\mathbf{F}_g\right) - \mathbf{S}(\boldsymbol{\omega}){}^{B}\mathbf{v} - \frac{\dot{m}}{m}{}^{B}\mathbf{v}. \tag{9} $$

The last term of (9) can be discarded because for LVs $\frac{\dot{m}}{m} << 1$. Hence, it is small when compared with other terms.

Separating (9) into scalar components and solving in order to the linear acceleration:

$$ \begin{cases} \dot{u} &= \frac{Tc\delta_y c\delta_p - (Dc\beta c\alpha + Ls\beta c\alpha)}{m} - gc\theta c\psi + rv - qw \\ \dot{v} &= \frac{T\sqrt{2}}{2}\frac{\left(s\delta_y + c\delta_y s\delta_p\right) + (Lc\beta - Ds\beta)}{m} - g\left(s\phi s\theta c\psi - c\phi s\psi\right) \\ &\quad + pw - ru \\ \dot{w} &= \frac{T\sqrt{2}}{2}\frac{\left(c\delta_y s\delta_p - s\delta_y\right) - (Ls\beta s\alpha + Dc\beta s\alpha)}{m} - g\left(c\phi s\theta c\psi + s\phi s\psi\right) \\ &\quad + qu - pv. \end{cases} \tag{10} $$

For the rotational motion, starting from Euler's equation:

$$ \mathbf{M}_{CM} = \mathbf{I}\dot{\boldsymbol{\omega}} + \boldsymbol{\omega} \times \mathbf{I}\boldsymbol{\omega} \tag{11} $$

where $\mathbf{M}_{CM}$ represents the sum of external moments around the center of mass. The only forces that generate torques on the launcher are the thrust and aerodynamic forces. Euler's equation can be used, even though this is not a rigid body, since the temporal variation of the position of the center of mass is small [13]. The total moment acting on the body is:

$$ \begin{aligned} \sum \mathbf{M}_{CM} &= \mathbf{l}_{GA} \times {}^{B}\mathbf{F}_a + \mathbf{l}_{CG} \times {}^{B}\mathbf{T} \\ &= \begin{bmatrix} 0 \\ \frac{\sqrt{2}}{2}Tl_{CG}\left(c\delta_y s\delta_p - s\delta_y\right) + \left(Dc\beta s\alpha + Ls\beta s\alpha\right) l_{GA} \\ -\frac{\sqrt{2}}{2}Tl_{CG}\left(c\delta_y s\delta_p + s\delta_y\right) + \left(Lc\beta - Ds\beta\right) l_{GA} \end{bmatrix}. \end{aligned} \tag{12} $$

where $\mathbf{l}_{GA} = (\mathbf{X}_{CP} - \mathbf{X}_g)$ represents the lever arm between the center of pressure and the center of gravity and $\mathbf{l}_{CG} = (\mathbf{X}_g - \mathbf{X}_{PVP_T})$ represent the lever arm between the center of gravity and the pivot point of the thrust vector. Noting that the body-axes are principal axes of inertia and that the launch vehicle is symmetrical, then $Ixy = Ixz = 0$. Hence the inertia tensor is simply

$$ \mathbf{I} = \begin{bmatrix} I_{xx} & 0 & 0 \\ 0 & I_{yy} & 0 \\ 0 & 0 & I_{zz} \end{bmatrix}. \tag{13} $$

Furthermore, due to the geometry of the LV, it is known that $I_{yy} = I_{zz} \gg I_{xx}$.

Developing equation (11) with (12) and (13) and solving w.r.t. to the angular acceleration yields:

$$ \begin{cases} \dot{p} = 0 \\ \dot{q} = \frac{\frac{\sqrt{2}}{2}Tl_{CG}\left(c\delta_y s\delta_p - s\delta_y\right) l_{CG} + \left(Dc\beta s\alpha + Ls\beta s\alpha\right) l_{GA}}{I_{yy}} - \frac{I_{xx} - I_{zz}}{I_{yy}} pr \\ \dot{r} = \frac{-\frac{\sqrt{2}}{2}Tl_{CG}\left(c\delta_y s\delta_p + s\delta_y\right) + \left(Lc\beta - Ds\beta\right) l_{GA}}{I_{zz}} - \frac{I_{xx} - I_{yy}}{I_{zz}} pq. \end{cases} \tag{14} $$

From (14) it is clear that the pitch and yaw dynamics are coupled in the presence of the roll-rate, p, as discussed earlier. Furthermore, if $p = 0$, pitch and yaw dynamics are independent and can be treated separately. In the nominal conditions, $\dot{p} = 0$ and the roll-rate p will be very small, so the dynamics of q and r can be simplified.

Given that this is a mass-varying system and the value of the mass at each step in time is a parameter for the other states, its dynamics must be defined. The initial mass of the system is $m(0) = 137820$ kg. The propellant mass for the first stage is $M_{\text{prop}} = 88383$ kg [8]. The mass flow rate is constant and only due to the exhausted propellant, hence $\dot{m} \approx$ constant. The separation of the first stage of the vehicle occurs approximately 100 s after launch, so $\dot{m} \approx \frac{\text{mprop}}{t_{\text{sep}}} = 900$ kg/s. Hence, the differential equation that regulates the exhaustion of mass in time is given by:

$$ \dot{m} = -900,\ m(0) = 137820 \text{ kg}. \tag{15} $$

Flexible modes modelling

As discussed in Section I, the flexible modes are very important for the design of the control system of a launch vehicle. The most straightforward way to include their contribution in the model is to assume that due to bending an extra force and moment is generated and must be added to the total forces and moments. It is also assumed that the lateral vibrations along the y_B-axis are the most relevant. These vibrations are caused by the component of the thrust force acting on the y_B-axis. Therefore, the additional force caused by the flexible modes shall be applied in this axis, while the additional moment appears in the z_B-axis. The equations of the flexible modes are:

$$ \begin{cases} \ddot{q}_i = -\omega_i^2 q_i - 2\xi\omega_i\dot{q}_i - T_y t_{pi} \\ F_{\text{flex}_y} = T_y \cdot \sum_{i=1}^{N} r_{pi} q_i \qquad\qquad , i = 1, 2 \\ M_{\text{flex}_z} = T_y \cdot \sum_{i=1}^{N} \left(r_{pi} \cdot l_{CG} + t_{pi}\right) q_i \\ \mathbf{F}_{\text{flex}} = \begin{bmatrix} 0 & F_{\text{flex}_y} & 0 \end{bmatrix}^T \\ \mathbf{M}_{\text{flex}} = \begin{bmatrix} 0 & 0 & M_{\text{flex}_z} \end{bmatrix}^T. \end{cases} \tag{16} $$

The full nonlinear 6 Degree of Freedom (DoF) dynamic model of a general LV is given by (2), (10), (14), (15) and, (16), describing respectively the Euler angle dynamics, linear acceleration, angular acceleration, mass exhaust rate, flexible modes states and force and moment induced by the flexible modes. Joining all the information from the previous equations, the full nonlinear model is defined in (17).

$$ f(\mathbf{x}, \mathbf{u}, t) = \begin{cases} {}^{B}\dot{\mathbf{v}}_B = \frac{1}{m} \cdot \sum \mathbf{F}_{\text{ext}} - \mathbf{S}\left({}^{B}\boldsymbol{\omega}_B\right){}^{B}\mathbf{v}_B \\ {}^{B}\dot{\boldsymbol{\omega}}_B = I^{-1}\left(\sum \mathbf{M}_{\text{ext}} - {}^{B}\boldsymbol{\omega}_{\boldsymbol{B}} \times \mathbf{I} \cdot {}^{B}\boldsymbol{\omega}_B\right) \\ \dot{\boldsymbol{\lambda}}_B = f_0\left(\boldsymbol{\lambda}\right) \cdot {}^{B}\boldsymbol{\omega}_B \\ \dot{m} = -900 \text{ kg/s} \\ \ddot{q}_i = -\omega_i^2 q_i - 2\xi\omega_i\dot{q}_i - T_y t_{pi},\ i = 1, 2 \\ {}^{L}\dot{\mathbf{P}}_B = {}^{L}_{B}\mathbf{R}\,{}^{B}\mathbf{v}_B. \end{cases} \tag{17} $$

Using this model it is possible to design different algorithms to control the LV, which is the topic of the next Sections.

III. Linear control

Trimming and Linearization

The model presented in Equation (17) can be trimmed and linearized around a reference trajectory, yielding a linear models suitable for control. For linearization, rigid-body motion (without flexible modes) is considered. Linearization is performed with frozen parameters around the trim points in the reference trajectory. In order to obtain valid trim points the following assumptions are considered:

- Rigid-body model;
- Movement occurs in the $x_b y_b$-plane $\rightarrow w = 0$;
- Roll angle is null, $\phi = 0$.

After trimming and linearization a 10 states state-space model is obtained, for each linearization point. Linearization was performed every second from $t = 0$ s to $t = 60$ s, yielding 60 linear systems describing the evolution of the nonlinear system in time. The state vector after trimming and linearization is $\mathbf{x} = [u\ v\ w\ p\ q\ r\ \phi\ \theta\ \psi\ m]^T$.

Analysis of the poles of the linearized systems

A LV is inherently unstable because its center of gravity lies aft of the center of pressure, hence a control system is always necessary. Given that the LV's mass is variable, there is no guarantee that a controller designed for a specific trim point can stabilize the system for all trim conditions. As such, it is useful to have insight on the evolution of the poles with time. To simplify this analysis, the model is decoupled into a longitudinal and a lateral model. Due to the axial symmetry of the launch vehicle, and given that in trim points the roll angle is null, this assumption is valid [9].

Defining $\mathbf{x_{long}} = [u\ v\ r\ \psi]^T$ as the longitudinal state and $\mathbf{x_{lat}} = [w\ p\ q\ \theta]^T$ as the lateral state, it is possible to separate the linearized model, while maintaining essential information about the dynamics. Note that the mass is not included in any of the models because it is independent of all the other states and does not influence the analysis in terms of control. As such, mass is considered a frozen parameter for each linearization point. Furthermore, the roll angle is not a state in any of the systems, as it is considered to be small and does not influence the dynamics of the lateral or longitudinal systems.

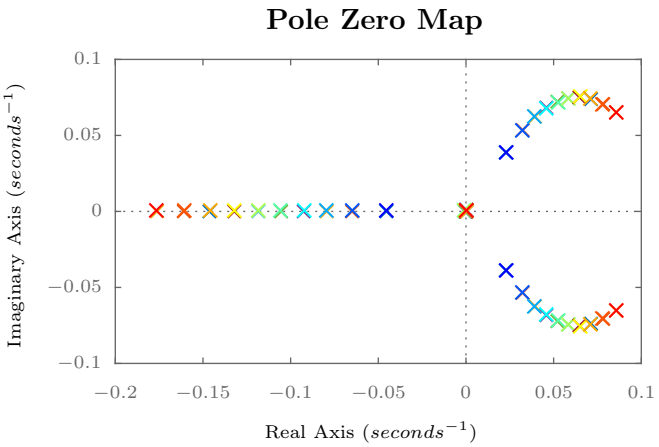

Fig. 2: Longitudinal poles associated with state variables $[u\ v\ r\ \psi]$

Figure 2 shows the evolution of the poles of the longitudinal models from $t = 0$ s to $t = 10$ s. In the figure, the first ten linearized models are shown. The color of the poles vary from blue to red, from the first to the last model, respectively. The evolution of the lateral poles is extremely similar hence it is not shown. Analysing the rest of the linearized models some conclusions can be drawn about the evolution of the linearized models:

- Due to the symmetry of the vehicle, the decoupled longitudinal and lateral models are extremely similar;
- The system is inherently unstable, as there are always poles in the right-half plane;
- Up until t=30s there are unstable complex poles;
- As times increases, the system becomes faster, since the magnitude of the poles increase.

Having insight about the evolution of poles of the model with time, controllers for the model are developed next.

LQR control

To allow tracking of the reference Euler angles, a LQR controller using the angular velocities and Euler angles is conducted, feeding the states $[q\ r\ \theta\ \psi]$ to the controller. Remember that there is no active actuation on the x_B-axis, hence the roll angle (ϕ) and angular velocity (p) are not controlled.

To facilitate the tuning of the controller, first order high pass filters are placed in the control variables, $[\delta_p\ \delta_y]$ and (first order) low pass filter are placed in the Euler angle states. The resulting system for the synthesis of the LQR controller has 8 states, $\left[\delta_{p_{effort}}\ \delta_{y_{effort}}\ lp_\theta\ lp_\psi\ q\ r\ \theta\ \psi\right]$, that will be fed to the controller. Varying the filter coefficients in the Q matrix in LQR synthesis it is possible to access its impact. The filter's effect can be summarised as follows:

High pass filter (control effort weight) - this filter is applied to the control variables and prevents high frequency content in the control signal. Increasing the importance of this filter in the Q-matrix leads to a decrease of the control signal RMS but to an increase in the tracking error RMS, showing a trade-off between these two parameters.

Low pass filter (performance weight) - filtering the reference signal reduces the sensitivity of the controller to abrupt variations (and noise) in the reference signal. Emphasizing the effect of this filter in the Q-matrix lead to a decrease in the tracking error (as abrupt variations are ignored) but the control signal RMS increases.

The coefficients of the filters are chosen such that the the controller is able to follow the reference while being robust to noise and limiting the high frequency in the response.

Along with the LQR controller, two SISO PID controllers (one each decoupled model) were developed. With the PID approach it was possible to stabilize the system, but the performance was considerably worse than the LQR controller. Hence, its implementation is not discussed here. Nonetheless, Table I shows a comparison of the response of the LQR and PID controllers to a 1 ° step in the pitch angle.

	LQR	PID
Rise Time (s)	0.3604	0.1228
Settling Time (s)	0.6270	2.0303
Overshoot (%)	0.1409	55.2670
δ_{pRMS}	0.6530	1.8575

TABLE I: Comparison of PID and LQR response

From table I, it is clear that using a state feedback method such as LQR is more advantageous than using two PIDs for the decoupled lateral and longitudinal models, as the settling time, overshoot and control action RMS are much better with LQR control. This comparison was carried out using the full linearized model at $t = 10$ s (for which both controllers were designed) and including the actuator model. The actuators are modelled as a second order low pass filter, with the transfer function [23], [24] shown in Eq. (18).

$$\frac{\delta_{real}}{\delta_{commanded}}(s) = \frac{\omega_{act}^2}{s^2 + 2\zeta_{act}\omega_{act}s + \omega_{act}^2}. \tag{18}$$

The LQR controller is able to stabilize the system for all trim points. Furthermore, applying this controller to the nonlinear system yields good results in the nominal conditions, as it is possible to track the reference trajectory. Next the robustness analysis of the LQR controller to parameter variation is assessed.

Robustness analysis of the LQR controller

A well designed controller must be robust to uncertainties in system parameters. This is especially relevant for LVs, given its critical application. Thus far, for linear control design, it was considered that the parameters of the system were "frozen" at the trim points. Given that the parameters of the system vary considerably in time, it is important to guarantee that the controller is able to cope with changes around the nominal values of said parameters.

At this point, it is important to clarify why many of parameters of the system are time-varying and its magnitude have a considerable variation. The system looses mass at a constant rate of $\dot{m} = 900\ kg/s$. Hence, all the parameters associated with mass distribution also change, namely, the position of the center of gravity ($\mathbf{X}_{CG}$), moments of inertia (I_{xx}, I_{yy} and I_{zz}) and obviously mass (m). Variation of the aerodynamic coefficients (C_a, C_n) will also be considered, although they are not directly related with the loss of mass.

Furthermore the effect of varying geometric parameters such as the position of the nozzle pivot point ($\mathbf{X}_{PVP}$) and the reference aerodynamic surface of the rocket, S are also considered.

For each of these parameters, its value will be changed $\pm 20\%$ around their nominal value. The nominal value of the time-varying parameters is considered as the trim value at $t = 10\ s$, to be consistent with previous sections. I_{yy} has the most important influence in the behaviour of the system. This analysis was performed for all aforementioned parameters, however, to improve readability, only I_{yy} is detailed here. Table II shows the effect of varying I_{yy} around its nominal value.

	$0.8I_{yy}$	$0.9I_{yy}$	I_{yy}	$1.1I_{yy}$	$1.2I_{yy}$
Rise Time (s)	0.39	0.37	0.36	0.35	0.35
Settling Time (s)	0.74	0.68	0.62	0.58	0.57
Overshoot (%)	0.00	0.00	0.22	1.08	2.27
$\delta_{p_{\text{RMS}}}$	0.60	0.63	0.66	0.68	0.71
$(\theta_{ref} - \theta)_{\text{RMS}}$	0.19	0.19	0.20	0.20	0.20

TABLE II: Summary of the effect of varying I_{yy} in the system's response to a step in θ

Decreasing I_{yy} makes the system faster. On the other hand, increasing I_{yy} shows the opposite trend: increase in overshoot and control action RMS and decrease in rise time and settling time. With the previous analysis, one can conclude that even with a 20% change in the nominal parameter, the controller is able to stabilize the system and the control signal does not exceed the saturation limit.

IV. Nonlinear control

Nominal design

This section is devoted to the implementation of a nonlinear backstepping controller for the LV. The control objective defined in Section II is to follow a reference trajectory expressed through the Euler angles, hence to ensure that $\boldsymbol{\lambda} \to \boldsymbol{\lambda}_d$. Equivalently, this can be written in terms of the reference tracking error, $\tilde{\boldsymbol{\lambda}} = \boldsymbol{\lambda} - \boldsymbol{\lambda}_d$, with the objective $\tilde{\boldsymbol{\lambda}} \to 0$.

As seen before, there is no actuation along the x-axis, hence the roll angle cannot be controlled. Thus the control objective can be defined as a function of the two controllable angles. Defining the controlled angles as $\boldsymbol{\lambda}_c = [\theta\ \psi]^T$ and the controlled angular velocity as $\boldsymbol{\omega}_c = [q\ r]^T$, the control objective can be stated as $\tilde{\boldsymbol{\lambda}}_c \to 0$.

The term $\sum M_{\text{ext}}$ can be written such that the dependence on the input variables is clear. From (12), there is symmetry in the control input term associated with the moment generated by the TVC system. Defining $c_1 = \frac{\sqrt{2}}{2} T l_{CG}$, $u_q = c\delta_y s\delta_p - s\delta_y$, $u_r = c\delta_y s\delta_p + s\delta_y$, $A_q = (Dc\beta s\alpha + Ls\beta s\alpha)\, l_{GA}$ and $A_r = (Lc\beta - Ds\beta)\, l_{GA}$:

$$\sum \mathbf{M}_{\text{ext}} = A + Bu,\ \text{with}\ \mathbf{A} = \begin{bmatrix} A_q \\ A_r \end{bmatrix}, \quad \mathbf{B} = \begin{bmatrix} c_1 & 0 \\ 0 & -c_1 \end{bmatrix},\ \mathbf{u} = \begin{bmatrix} u_q \\ u_r \end{bmatrix}. \tag{19}$$

In the nominal model $\dot{p} = 0$, hence the cross-coupling terms from the cross product $\omega_c \times I\omega_c$ are zero. Cases were $\dot{p} \neq 0$, will be considered as a perturbation to the nominal model and will be treated in subsequent sections.

Substituting Eq. (19) into (17) yields a model in strict-feedback form:

$$\begin{cases} \dot{\lambda}_c &= f_0\left(\phi, \theta\right) \cdot \omega_c \\ \dot{\omega}_c &= I_c^{-1}\left(A + Bu\right). \end{cases} \tag{20}$$

The controlled Euler angles error dynamics can be defined as:

$$\dot{\tilde{\lambda}}_c = \dot{\lambda}_c - \dot{\lambda}_{c_d} = f_0(\phi, \theta)\omega_c - \dot{\lambda}_{c_d}. \tag{21}$$

Regarding the controlled angular velocity, ω_c, as the control input for the $\dot{\tilde{\lambda}}_c$ system, the desired control can be defined as:

$$\omega_{c_d} = \alpha\left(\lambda_c, \lambda_{c_d}, \dot{\lambda}_{c_d}\right). \tag{22}$$

It is possible to define a Lyapunov function using the Euler angles error to assess the stability of the system:

$$V_1(\tilde{\lambda}_c) = \frac{1}{2}\tilde{\lambda}_c^T \tilde{\lambda}_c. \tag{23}$$

To guarantee stability, the Lyapunov function must be positive-definite and its derivative negative-definite. Checking the requirement of positive-definiteness for V_1:

- $V_1(\tilde{\lambda}_c = 0) = 0$;
- $V_1(\tilde{\lambda}_c) > 0\ \forall \tilde{\lambda}_c \neq 0$, because V_1 is a quadratic function.

The derivative of the Lyapunov function, (23) is

$$\dot{V}_1(\tilde{\lambda}_c) = \tilde{\lambda}_c^T \dot{\tilde{\lambda}}_c = \tilde{\lambda}_c^T \left[f_0(\phi, \theta)\omega_c - \dot{\lambda}_c\right]. \tag{24}$$

Now, substituting (22) in (24):

$$\dot{V}_1(\tilde{\lambda}_c) = \tilde{\lambda}_c^T \left[f_0(\phi, \theta)\alpha\left(\lambda_c, \lambda_{c_d}, \dot{\lambda}_{c_d}\right) - \dot{\lambda}_c\right] \leq -W_1\left(\tilde{\lambda}_c\right). \tag{25}$$

Choosing α such that $\dot{V}_1(\tilde{\lambda}_c) \leq -W_1(\tilde{\lambda}_c)$, where $W_1(\tilde{\lambda}_c)$ is a positive definite function of the reference tracking error, guarantees stability. From (25), a suitable choice for α can be deduced, provided that $f_0(\phi, \theta)$ is invertible.

Choosing $\alpha\left(\lambda_c, \lambda_{c_d}, \dot{\lambda}_{c_d}\right) = -f_0(\lambda_c)^{-1}\left(K_{ang}\tilde{\lambda}_c - \dot{\lambda}_{c_d}\right)$, yields

$$\dot{V}_1(\tilde{\lambda}_c) = -\tilde{\lambda}_c^T K_{ang} \tilde{\lambda}_c < 0, \quad \forall K_{ang} > 0, \tag{26}$$

where K_{ang} is a diagonal matrix. The inverse of matrix $f_0(\phi, \theta)$ is given by:

$$f_0(\phi, \theta) = \begin{bmatrix} \cos\phi & -\sin\phi \\ \sin\phi/cos\theta & \cos\phi/\cos\theta \end{bmatrix}, \quad f_0(\phi, \theta)^{-1} = \begin{bmatrix} \cos\phi & \sin\phi\cos\theta \\ -\sin\phi & \cos\phi\cos\theta \end{bmatrix}. \tag{27}$$

To proceed with backstepping design, $\tilde{\omega}_c = \omega_c - \omega_{c_d}$ is defined as the angular velocity error. Rewriting the original system in terms of the tracking and angular velocity errors:

$$\begin{cases} \dot{\tilde{\lambda}}_c = f_0(\phi, \theta)\tilde{\omega}_c - K_{\text{ang}}\tilde{\lambda}_c \\ \dot{\tilde{\omega}}_c = I_c^{-1}\left(A + Bu\right) - \dot{\alpha}(\lambda_c, \lambda_{c_d}, \dot{\lambda}_{c_d}). \end{cases} \tag{28}$$

The derivative

$$\dot{\alpha}\left(\lambda_c, \lambda_{c_d}, \dot{\lambda}_{c_d}\right) = \dot{\omega}_{c_d} = \frac{d}{dt} f_0^{-1}(\phi(t), \theta(t)) \cdot \left(K_{\text{ang}}\tilde{\lambda}_c - \dot{\lambda}_{c_d}\right) - f_0^{-1}(\phi(t), \theta(t)) \cdot \frac{d}{dt}\left(K_{\text{ang}}\tilde{\lambda}_c - \dot{\lambda}_{c_d}\right). \tag{29}$$

The first parcel can be written as a function of the Euler angles and angular velocities:

$$\frac{d}{dt} f_0^{-1}(\phi(t), \theta(t)) = \underbrace{\begin{bmatrix} -s^2\phi t\theta & 0 \\ -c\phi s\phi t\theta & -s\theta \end{bmatrix} q + \begin{bmatrix} -s\phi c\phi t\theta & s\theta \\ -c^2\phi t\theta & 0 \end{bmatrix} r}_{F(\phi,\theta,q,r)} \tag{30}$$

The second parcel can be written using previous definitions. The total expression for the derivative is given in Eq. (31).

$$\dot{\omega}_{c_d} = F(\phi, \theta, q, r)\left(K_{\text{ang}}\tilde{\lambda}_c - \dot{\lambda}_{c_d}\right) + f_0^{-1}\left(\ddot{\lambda}_{c_d} - K_{\text{ang}}\dot{\tilde{\lambda}}_c\right) \tag{31}$$

Now, defining a composite Lyapunov function for the whole system as

$$V_2(\tilde{\lambda}_c, \tilde{\omega}_c) = V_1(\tilde{\lambda}_c) + \frac{1}{2}\tilde{\omega_c}^T\tilde{\omega_c} \tag{32}$$

The derivative of the candidate Lyapunov function is

$$\dot{V}_2(\tilde{\lambda}_c, \tilde{\omega}_c) = -\tilde{\lambda}_c^T K_{\text{ang}}\tilde{\lambda}_c + \tilde{\omega}_c^T I_c^{-1}\left[I f_0(\phi, \theta)\tilde{\lambda}_c + A + Bu - I_c\dot{\omega}_{c_d}\right]. \tag{33}$$

Finally, choosing u such that the derivative of the Lyapunov function, $\dot{V}_2(\tilde{\lambda}, \tilde{\omega})$ is negative definite, stability for the whole system is guaranteed. Choosing

$$u = -B^{-1}\left(I_c f_0(\phi, \theta)^T\tilde{\lambda}_c + A + I_c\left(K_\omega\tilde{\omega}_c - \dot{\omega}_{c_d}\right)\right), \tag{34}$$

then the derivative of the Lyapunov function becomes

$$\dot{V}_2(\tilde{\lambda}_c, \tilde{\omega}_c) = -\tilde{\lambda}_c^T K_{\text{ang}}\tilde{\lambda}_c - \tilde{\omega}_c^T K_w\tilde{\omega}_c < 0, \ \ \forall K_{\text{ang}} > 0, \ K_\omega > 0. \tag{35}$$

There are two gain matrices, K_{ang} and K_w that can be adjusted to tune the controller response. Furthermore, for the nominal system, it arises from the Lyapunov stability analysis that the only requirement to ensure stability is that both gain matrices are positive-definite. Matrix B is invertible because it is a real diagonal matrix and its inverse is given by

$$B^{-1} = \begin{bmatrix} 1/c_1 & 0 \\ 0 & -1/c_1 \end{bmatrix}. \tag{36}$$

The control law determined in (34) stabilizes the system in nominal conditions. Next, robustness to parameter uncertainties will be studied.

Robustness analysis of the nonlinear controller

The analysis will be carried on through modelling a particular disturbance and then using the Lypunov function to obtain relations between the gains, magnitude of the errors and parameters of the system. Two cases are presented here: robustness to bounded roll-rate disturbances and robustness to uncertainty in the position of the center of mass. These two cases show two different methodologies to assess robustness, the theoretical approach using the Lyapunov function and a simulation approach. More cases were studied but these two are representative of the methodologies employed.

Robustness to bounded roll-rate disturbances

As discussed earlier, in this stage of the mission, the roll-rate is not actively controlled, as there is a roll-rate limiter that acts if $|p| > 45$ °/s. [8], [11], [25]. Therefore, the system must be stable for disturbances up to this value.

In the presence of roll-rate, the pitch and yaw dynamics are given by:

$$\begin{cases} \dot{q} = \frac{1}{I_{yy}}\left(A_q + c_1 u_q - (I_{xx} - I_{zz})\, pr\right) \\ \dot{r} = \frac{1}{I_{zz}}\left(A_r - c_1 u_q - (I_{xx} - I_{yy})\, pq\right). \end{cases} \tag{37}$$

Rewriting the error dynamics of the controlled angular velocity in matrix form:

$$\dot{\tilde{\omega}}_c = I_c^{-1}\left(A + Bu + P\omega_c\right) - \dot{\omega}_{c_d}, \tag{38}$$

where P is the perturbation to the state introduced by the non-null roll-rate and A and B are the matrices defined in (19):

$$P = \begin{bmatrix} 0 & (I_{zz} - I_{xx})p \\ (I_{yy} - I_{xx})p & 0 \end{bmatrix}. \tag{39}$$

Now using (38) and the nominal control deduced in the (34), the derivative of the Lyapunov function can be reformulated. Building on previous results and using the relation $\omega_c = \tilde{\omega}_c + \omega_{c_d}$:

$$\dot{V}_2(\tilde{\lambda}_c, \tilde{\omega}_c) = -\tilde{\lambda}_c^T K_{\text{ang}}\tilde{\lambda}_c - \tilde{\omega}_c I_c^{-1}\left[I_c f_0(\phi, \theta) + A + Bu - I_c\dot{\omega}_{c_d} + P\tilde{\omega}_c + P\omega_{c_d}\right]. \tag{40}$$

Substituting the nominal control, Eq. (34), and collecting the terms:

$$\dot{V}_2(\tilde{\lambda}_c, \tilde{\omega}_c) = -\tilde{\lambda}_c^T K_{\text{ang}}\tilde{\lambda}_c - \tilde{\omega}_c^T(K_w - I_c^{-1}P)\tilde{\omega}_c - \underbrace{\tilde{\omega}_c^T I_c^{-1} P f_0^{-1} K_{\text{ang}}}_{\mathbf{x}^T}\underbrace{\tilde{\lambda}_c}_{\mathbf{y}} + \tilde{\omega}_c^T I_c^{-1} P f_0^{-1}\dot{\lambda}_{c_d}. \tag{41}$$

The first term is negative-definite by construction, because $K_{\text{ang}} \succ 0$. The second term is negative definite if $K_w - I_c^{-1}P \succ 0$. The third term is a cross term between $\tilde{\lambda_c}$ and $\tilde{\omega_c}$, so using Young's inequality (with $\mathbf{x}$ and $\mathbf{y}$ as defined in Eq. (41)) it can be written as:

$$\tilde{\omega}_c^T I_c^{-1} P f_0^{-1} K_{\text{ang}}\tilde{\lambda}_c < \frac{1}{2}\tilde{\omega}_c^T T\tilde{\omega}_c + \frac{1}{2}\tilde{\lambda}_c^T\tilde{\lambda}_c \tag{42}$$

Substituting Eq. (42) in (41) and using the definition $\tilde{\mathbf{x}} = \begin{bmatrix}\tilde{\lambda}_c & \tilde{\omega}_c\end{bmatrix}^T$:

$$\dot{V}_2(\tilde{\mathbf{x}}) < -\tilde{\mathbf{x}}^T M\tilde{\mathbf{x}} + \tilde{\mathbf{x}}^T N\dot{\lambda}_{c_d}, \tag{43}$$

where $M = \begin{bmatrix} K_{\text{ang}} - \frac{1}{2}I & 0 \\ 0 & K_w - I_c^{-1}P - \frac{1}{2}T \end{bmatrix}$, $N = \begin{bmatrix} 0 \\ I_c^{-1}P \end{bmatrix}$.

From (43) it can be concluded that the system is input-to-state stable, meaning that for any bounded input (in this case $\dot{\lambda}_{c_d}$), the norm of $\tilde{\mathbf{x}}$ will be bounded. To show that the system is input-to-state stable, the conditions for having $\dot{V}_2 < 0$ must be determined. Hence,

$$\tilde{\mathbf{x}}^T M\tilde{\mathbf{x}} > \tilde{\mathbf{x}}^T N\dot{\lambda}_{c_d} \tag{44}$$

For a positive-definite matrix M, using the Rayleight-Ritz inequality:

$$\tilde{\mathbf{x}}^T M\tilde{\mathbf{x}} \geq \lambda_{\min}(M)\tilde{\mathbf{x}}^T\tilde{\mathbf{x}} > ||\tilde{\mathbf{x}}||\lambda_{\max}(I_c^{-1}P)||\dot{\lambda}_{c_d}|| \Rightarrow ||\tilde{\mathbf{x}}|| > \frac{\lambda_{\max}(I_c^{-1}P)}{\lambda_{\min}(M)}||\dot{\lambda}_{c_d}|| \tag{45}$$

It follows that if the norm of $\dot{\lambda}_{c_d}$ is bounded, then the norm of $||\tilde{\mathbf{x}}||$ remains bounded and the system is input-to-state stable. Essentially, if the modulus of the error is larger than a given bound, the derivative of the Lyapunov function is negative and the system is stable. If the error is smaller than this bound, there is no guarantee on the signal of $\dot{V}_2(\tilde{\mathbf{x}})$ but it is guaranteed that the error remains inside the level set $||\tilde{\mathbf{x}}|| < \frac{\lambda_{\max}(I_c^{-1}P)}{\lambda_{\min}(M)}||\dot{\lambda}_{c_d}||$.

M is positive-definite if its eigenvalues are all real and positive. Given that M is a block diagonal matrix, with zeros in the off-diagonal terms, using Schur's complement condition for positive-definiteness, M is positive definite if and only if $K_{\text{ang}} - \frac{1}{2}I \succ 0$ and $K_w - I_c^{-1}P - \frac{1}{2}T \succ 0$. The first condition is meet if

$$\begin{cases} K_\theta > 0.5 \\ K_\psi > 0.5 \end{cases} \tag{46}$$

The second condition can be written as $K_w > \underbrace{I_c^{-1}P + \frac{1}{2}T}_{Q}$. Assuming that $K_\theta = K_\psi$, then $K_{\text{ang}} = K_\theta I$ and $T = K_\theta^2 I_c^{-1} P f_0^{-1} I f_0^{-T} (I_c^{-1}P)^T$. Furthermore, writing

$$f_0^{-1} f_0^{-T} = \begin{bmatrix} a & -c \\ -c & b \end{bmatrix}, \; I_c^{-1}P = K_I \begin{bmatrix} 0 & 1 \\ 1 & 0 \end{bmatrix}, \tag{47}$$

where $K_I = \frac{I_{zz} - I_{xx}}{I_{zz}} p$. Noting that $K_I > 0$, then the eigenvalues of $I_c^{-1}P$ are always real and positive. Thus Q can be written as:

$$Q = \begin{bmatrix} \frac{1}{2}K_\theta^2 K_I^2 b & K_I - \frac{1}{2}K_\theta^2 K_I^2 c \\ K_I - \frac{1}{2}K_\theta^2 K_I^2 c & \frac{1}{2}K_\theta^2 K_I^2 a \end{bmatrix} \tag{48}$$

Q is symmetric and positive-definite. Using the Rayleigh-Ritz inequality for an arbitrary $n \times 1$ real vector, $\mathbf{x}$ (in order to majorate this matrix and cover the worst case scenario):

$$\begin{cases} \lambda_{\min}(K_w)\mathbf{x}^T\mathbf{x} \leq \mathbf{x}^T K_w \mathbf{x} \leq \lambda_{\max}(K_w)\mathbf{x}^T\mathbf{x} \\ \lambda_{\min}(Q)\mathbf{x}^T\mathbf{x} \leq \mathbf{x}^T Q \mathbf{x} \leq \lambda_{\max}(Q)\mathbf{x}^T\mathbf{x} \end{cases} \tag{49}$$

Combining this, $K_w - Q \succ 0$ if:

$$\lambda_{\min}(K_w)\mathbf{x}^T\mathbf{x} > \lambda_{\max}(Q)\mathbf{x}^T\mathbf{x} \Rightarrow \lambda_{\min}(K_w) > \lambda_{\max}(Q) \tag{50}$$

Since $Q \geq 0$, then $||Q|| = \lambda_{\max}(Q)$. The trace of the matrix is bounded by $||Q|| \leq tr\ (Q) \leq n||Q||$, hence $\lambda_{\max}(Q) \leq tr\ (Q)$. Therefore to guarantee that M is positive-definite, $\lambda_{\min}(K_w) > tr\ (Q)$. From (48):

$$tr\ (Q) = \frac{1}{2}K_\theta^2 K_I^2 (1 + \underbrace{c^2\theta}_{0 \leq c^2\theta \leq 1}) \leq K_\theta^2 K_I^2 \tag{51}$$

Finally to guarantee positive-definiteness of M then $\lambda_{\min}(K_w) > K_\theta^2 K_I^2$. This relation is shown in Figure 3. In order to guarantee positive-definiteness of M, the minimum value of K_w must be above the blue line. Bear in mind that these are conservative values for the choice of gains, as they were obtained for the worst case scenario. It is guaranteed that if K_w is chosen with this criteria the system will be input-to-state stable. Lower values for these gains may also ensure stability, although no theoretical guarantee is given. Figure 3 does not show us the maximum error, as it only relates the minimum gain of K_w for each value of K_θ that guarantees positive-definiteness of M.

The condition on the maximum error is given by equation (45). This condition depends on the system trajectory because T depends on the Euler angles. Figure 4 shows a simulation of the system affected by a roll-rate disturbance of 45 °/s. On the left and right,

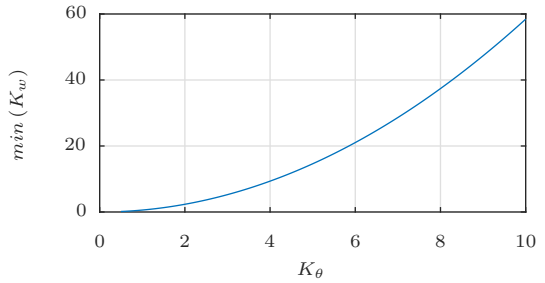

Fig. 3: Minimum value of K_w as a function of the gain of the outer loop, K_θ, for the maximum allowable roll-rate disturbance

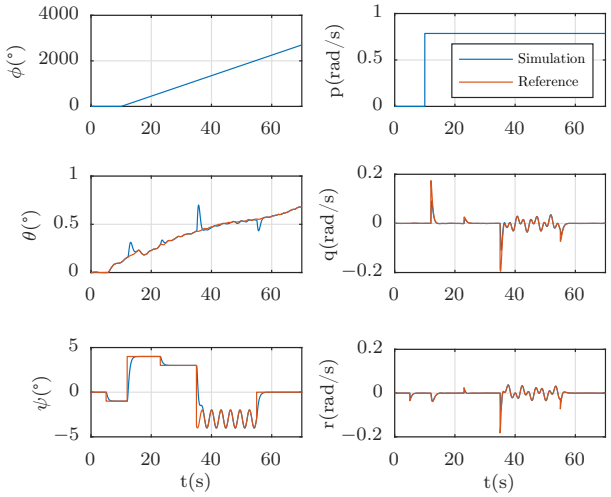

Fig. 4: Euler angles and angular velocity for a test trajectory with $K_w = 5 \cdot I$ and $K_{\text{ang}} = 2 \cdot I$ for $p = 45$°/s

the Euler angles and the angular velocities, with the reference in orange and simulated variables in blue. From this Figure one can see that the disturbance starts acting at $t = 10$ s and keeps acting until the end of the simulation. In the presence of a non-null roll-rate, there is a coupling between the motion in the y and z axis, which is evident for example around $t = 15$ s in Figure 4. The abrupt change in reference in ψ causes the tracking of θ to be degraded.

Robustness to uncertainty in the position of the center of mass, $\mathbf{P}_{CG}$

Forcing $\mathbf{P}_{\text{CG}}$ to be outside the x_B-axis generates moments in the other body axis that are not accounted for in the controller. Thus, even in the nominal case, the error increases with the uncertainty in the position of the center of mass. Having uncertainty in the position along x_B does not have a big impact on the system. It is also important to note that the effect of the uncertainty of the position of the center of mass varies with the considered trajectory. This analysis considers the nominal trajectory, for which the reference signal in ψ is more demanding than in θ. The analysis is the same for the three axis thus to avoid repetition only the analysis for uncertainty along the y_B-axis is detailed.

Considering a misalignment between the true position of the center of gravity and the modelled position of the center of gravity along the y-axis: $\mathbf{P}_{\text{CG}} = \mathbf{P}_{\text{CG}_N} + [0\ \delta_{\text{GC}_y}\ 0]$. This will generate moments in all axes. For a generic force, with components along the three body axes, the generated moment is given by (52).

$$\begin{bmatrix} l_{GA_x} \\ \delta_{\text{CG}_y} \\ 0 \end{bmatrix} \times \begin{bmatrix} F_x \\ F_y \\ F_z \end{bmatrix} = \begin{bmatrix} F_z \delta_{\text{CG}_y} \\ -F_z l_{GA_x} \\ F_y l_{GA_x} - F_x \delta_{\text{CG}_y} \end{bmatrix} \tag{52}$$

Due to this misalignment, there are two moments (one along the x axis and another along the z axis) that are not accounted for. Hence, they will not be compensated by the controller.

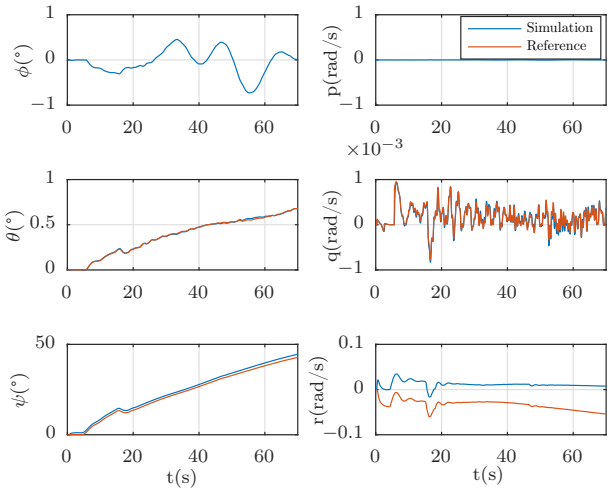

Fig. 5: System response with $\delta_{\text{GC}_y} = 0.4$ m

Figure 5 shows the response of the nominal system with an uncertainty of $\delta_{\text{GC}_y} = +0.4$ m in the location of the center of gravity along the y_B-axis. Although the system is still stable, the controller is not able to perfectly track the reference in r and ψ. There is a static error between the reference and the actual state. This difference occurs because the controller is using incomplete information to compute the control signal.

Adaptive backstepping control

One approach to mitigate the effect of uncertainty in the position of the center of mass is to estimate its true position and use this estimate in the backstepping controller design. The goal is to design and estimation law for the position of the center of mass and couple it with the previously designed controller. Consider that there is a misalignment (only) along the y_B-axis. If the misalignment occurred along the z_B-axis, the procedure described here would be the same. Furthermore, assume that the aerodynamic moments are known. Hence, the uncertainty will only affect the moment generated by the thrust force. In this case, the moments caused by the thrust force are:

$$\begin{bmatrix} l_{GA_x} \\ \delta_{\text{CG}_y} \\ 0 \end{bmatrix} \times \begin{bmatrix} T_x \\ T_y \\ T_z \end{bmatrix} = \begin{bmatrix} T_z \delta_{\text{CG}_y} \\ -T_z l_{GA_x} \\ T_y l_{GA_x} - T_x \delta_{\text{CG}_y} \end{bmatrix} \tag{53}$$

Recalling from Section II that $T_x = Tc\delta_y\delta_p$, the uncertainty introduced by the misalignment in the y_B-axis is a function of the input, thrust and the uncertainty itself. For the nominal trajectory, the control action is smooth and the control angles are limited by the actuators to $\pm 6.5^\circ$, thus the small angle approach is valid and $T_x \approx T$. Hence the moment induced by the perturbation is simply $T\delta_{\text{CG}_y}$. Introducing this in the dynamics of the angular velocity error:

$$\dot{\tilde{\omega}}_c = I_c^{-1} \left(A + Bu - I_c \dot{\omega}_{c_d} + \begin{bmatrix} 0 \\ T\delta_{\text{CG}_y} \end{bmatrix} \right) \tag{54}$$

The perturbation δ_{CG_y} is not known hence its estimate, $\hat{\delta}_{\text{CG}_y}$, must be used. Defining the estimation error as $\tilde{\delta}_{\text{CG}_y} = \delta_{\text{CG}_y} - \hat{\delta}_{\text{CG}_y}$, the estimate can replace the perturbation in (54), yielding

$$\dot{\tilde{\omega}}_c = I_c^{-1} \left(A + Bu - I_c \dot{\omega}_{c_d} + T\hat{\delta}_{\text{CG}_y} \begin{bmatrix} 0 \\ 1 \end{bmatrix} + T\tilde{\delta}_{\text{CG}_y} \begin{bmatrix} 0 \\ 1 \end{bmatrix} \right) \tag{55}$$

When defining the nominal backstepping controller, the control law u was such that all nonlinear terms are cancelled and a definite negative term in the Lyapunov function derivative is introduced. Now, the same is done, but also cancelling the term that depends on the estimated position of the center of mass. Then the Lyapunov function is used to determine a dynamic update law for $\hat{\delta}_{\text{CG}_y}$ that guarantees stability of the system. The new control law is given by:

$$u = -B^{-1} \left(\underbrace{I_c f_o(\phi,\theta)\tilde{\lambda_c} + A + I_c(K_w\tilde{\omega}_c - \dot{\omega}_{c_d})}_{u_N} - T\hat{\delta}_{\text{CG}_y} \begin{bmatrix} 0 \\ 1 \end{bmatrix} \right) \tag{56}$$

Augmenting the control Lyapunov function to include the estimation error:

$$V(\tilde{\lambda}_c, \tilde{\omega}_c, \tilde{\delta}_{\text{CG}_y}) = \frac{1}{2}\tilde{\lambda}_c^T\tilde{\lambda}_c + \frac{1}{2}\tilde{\omega}_c^T\tilde{\omega}_c + \frac{1}{2}\frac{1}{K_3}\tilde{\delta}_{\text{CG}_y}^2 \tag{57}$$

In equation (57), K_3 is a gain to control the dynamics of $\tilde{\delta}_{\text{CG}_y}$. The derivative of $\tilde{\delta}_{\text{CG}_y}$ is given by:

$$\dot{\tilde{\delta}}_{\text{CG}_y} = \underbrace{\dot{\delta}_{\text{CG}_y}}_{0} - \dot{\hat{\delta}}_{\text{CG}_y} \Rightarrow \dot{\tilde{\delta}}_{\text{CG}_y} = -\dot{\hat{\delta}}_{\text{CG}_y} \tag{58}$$

Using (58), the derivative of (57) can be written as:

$$\begin{aligned} \dot{V}(\tilde{\lambda}_c, \tilde{\omega}_c, \tilde{\delta}_{\text{CG}_y}) &= \dot{V}_2 + T\tilde{\delta}_{\text{CG}_y}\tilde{\omega_c}^T I_c^{-1} \begin{bmatrix} 0 \\ 1 \end{bmatrix} - \frac{1}{K_3}\tilde{\delta}_{\text{CG}_y}\dot{\tilde{\delta}}_{\text{CG}_y} \\ &= \dot{V}_{2_N} + \tilde{\delta}_{\text{CG}_y} \underbrace{\left(T\tilde{\omega_c}^T I_c^{-1} \begin{bmatrix} 0 \\ 1 \end{bmatrix} - \frac{1}{K_3}\dot{\tilde{\delta}}_{\text{CG}_y} \right)}_{=0} \end{aligned} \tag{59}$$

Using (59) the dynamics of $\dot{\hat{\delta}}_{\text{CG}_y}$ can be chosen such that the term multiplying $\tilde{\delta}_{\text{CG}_y}$ is zero:

$$\dot{\hat{\delta}}_{\text{CG}_y} = K_3 T\tilde{\omega}_c^T I_c^{-1} \begin{bmatrix} 0 \\ 1 \end{bmatrix} \tag{60}$$

Substituting Eq. (60) in the derivative of the new Lyapunov function, $\dot{V}(\tilde{\lambda}_c, \tilde{\omega}_c, \tilde{\delta}_{\text{CG}_y}) \leq 0$. Since $\dot{V}$ is only negative semi-definite and the system is nonautonomous, neither Lyapunov's second method nor LaSalle's Invariance Principle can be applied. However, Barbalat's Lemma can be applied, which ensures that $\dot{V}$ converges to zero, since V converges to a bounded limit and $\dot{V}$ is uniformly continuous. It follows that $\tilde{\lambda}_c$ and $\tilde{\omega_c}$ are guaranteed to converge to zero.

Now the backstepping controller incorporates a parameter estimation update law that stabilizes the system. Furthermore, gain K_3 allows some control over the speed of the convergence of the estimate of the true position of the center of gravity over the y_B-axis. It is important to note that given the implementation of the parameter estimation law using the Lyapunov function, the estimation error, $\tilde{\delta}_{\text{CG}_y}$, converges to a constant. However, it is not guaranteed that the estimate converges to the real value of the position of the center of mass. Figures 6 through 7b show the comparison of the nominal control and the adaptive control (with parameter estimation), for a misalignment of 0.7 m along the y_B-axis.

In Figure 6a, without the adaptive law, it is not possible to track the computed reference, because an unknown torque is acting upon the system, which is not taken into account when computing the control signal. In Figure 6b, with the adaptive control, the controller is now able to track the angular velocity reference. Examining Figure 7a, without adaptive control there is a static error in the reference tracking of ψ, which vanishes when using adaptive control.

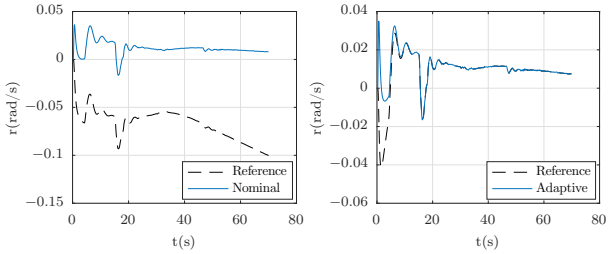

(a) Yaw rate using nominal control (b) Yaw rate using adaptive control

Fig. 6: Yaw rate for nominal and adaptive control with $\delta_{\text{CG}_y} = 0.7$ m

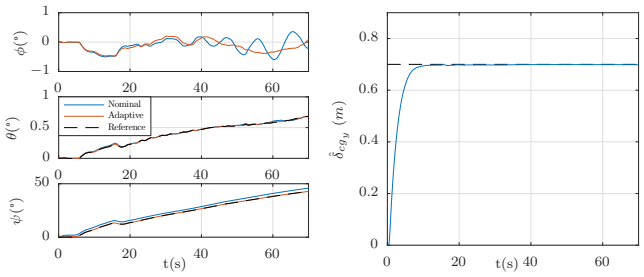

(a) Euler angles (b) Estimate $\hat{\delta}_{\text{CG}_y}$ with K_3=10

Fig. 7: Comparison of nominal and adaptive control for $\delta_{\text{CG}_y} = 0.7$ m

Figure 7b shows the evolution of the estimate $\hat{\delta}_{\text{CG}_y}$ with $K_3 = 10$. Approximately after 10 s the estimate converges to the real value of the deviation and the TVC system is able to counteract the extra moment induced by this deviation.

V. Comparison of the Linear and Nonlinear Controllers

It is one of the goals of this work to compare performance, advantages and drawbacks of using linear or nonlinear methods to control the atmospheric ascent of launch vehicles. Previously, it was seen that the LQR controller was much more robust than the PID controllers, hence only the performance of the LQR controller will be analysed.

By using nonlinear techniques, two controllers were developed: a nominal backstepping controller and an adaptive backstepping controller, with an adaptive control law to estimate the position of the center of mass. The benefits of the adaptive controller were seen in the previous section and relate to the specific case of uncertainty of the center of mass along the y_B-axis. Henceforth, to get a more general overview of linear vs. nonlinear control techniques applied to launchers, the adaptive backstepping controller is omitted from this comparison, although the conclusions can be extended for that case.

The performance of the LQR and backstepping controllers applied to the nonlinear model, for two different trajectories, both for nominal conditions and with flexible modes will be considered. The effect of flexible modes is considered a key factor that can destabilize the system, so this will be the disturbance considered in the present evaluation. The two trajectories used in the simulations are the nominal trajectory and a trajectory designed to test the flexible modes. Results are presented in Tables III and IV, respectively for the nominal trajectory and flexible modes trajectory.

Considering first Table III, it can be seen that the backstepping controller present smaller reference tracking errors, but the control action RMS is slightly higher. The overall results with both controllers for this trajectory are similar. The nominal trajectory is smooth and slowly varying, hence the flexible modes do not have a big impact on the system. In these conditions, the LQR controller achieves good performance and even though is it designed for the linearized model at $t = 10$ s, it is able to stabilize the nonlinear system. From Table IV it is clear that the performance of the LQR controller is degraded by the inclusion of the flexible modes. With both flexible modes this controller cannot stabilize the system, which is depicted by the exponential growth of the reference tracking error from nominal conditions to the inclusion of both flexible modes. On the other hand, the backstepping controller is able to stabilize the system with the flexible modes, with performance levels similar to the nominal case. Comparing the results of both trajectories, the performance of the backstepping degrades with respect to the nominal trajectory, but the controller is able to track the reference for all cases (with and without flexible modes). The LQR controller however behaves very poorly in the second considered trajectory with the flexible modes, as it cannot stabilize the system.

Therefore, the backstepping controller is more robust and yields better results than the LQR controller. Backstepping control is robust to changes in various parameters and uncertainties and can even be augmented with parameter estimation techniques in special circumstances.

		Nominal	1 flex	2 flex
LQR	$\sum \tilde{\theta}^2$	7.92E-05	7.92E-05	7.92E-05
	$\sum \tilde{\psi}^2$	0.1569	0.1569	0.1569
Backstepping	$\sum \tilde{\theta}^2$	1.90E-06	1.90E-06	1.90E-06
	$\sum \tilde{\psi}^2$	8.26E-05	8.26E-05	8.26E-05
LQR	$\delta_{p_{RMS}}$	0.00088	0.00089	0.00089
	$\delta_{y_{RMS}}$	0.00093	0.00094	0.00094
Backstepping	$\delta_{p_{RMS}}$	0.00099	0.00099	0.00100
	$\delta_{y_{RMS}}$	0.00104	0.00104	0.00105

TABLE III: Comparison of the LQR and backstepping, for the nominal trajectory

		Nominal	1 flex	2 flex
LQR	$\sum \tilde{\theta}^2$	0.225	0.3743	21.1322
	$\sum \tilde{\psi}^2$	6.8671	19.3424	561.6633
Backstepping	$\sum \tilde{\theta}^2$	0.2133	0.2124	0.2121
	$\sum \tilde{\psi}^2$	5.5623	5.0921	5.1652
LQR	$\delta_{p_{RMS}}$	0.0841	0.2188	1.3707
	$\delta_{y_{RMS}}$	0.0812	0.1887	0.9515
Backstepping	$\delta_{p_{RMS}}$	0.0261	0.0265	0.0279
	$\delta_{y_{RMS}}$	0.0242	0.0249	0.0265

TABLE IV: Comparison of LQR and backstepping, for the trajectory that excites the flexible modes

Given the results obtained with the LQR controller, one could think of designing a center of mass estimator, as developed for the backstepping controller. However, this is not straightforward due to several reasons. Firstly, this is a time-varying system and, as such, if using linear control, there are several controllers for each different part of the trajectory, with the switching done by a gain-scheduling algorithm. Hence, it is necessary to design several estimators (for the different parts of the trajectory). For backstepping control design this is not a problem, as the estimator dynamics are derived from the Lyapunov function and, therefore, are global (provided that global stability can be proven with the selected Lyapunov function). The

linear control techniques heavily rely on trim points (and therefore on the trajectory). If a controller is tuned for a particular trajectory, there is no guarantee that it will work properly for a different trajectory. For this reason, it is difficult to adapt the designed linear controllers to other LV. It is easier to adapt the backstepping controller to another launch vehicle, as the evaluation is based on Lyapunov stability analysis, which will be the same independently of the parameters of the system. What changes are the actual limits for the gains that ensure stability for the several considerer perturbations, as these are dependent on the trajectory and system parameters. To summarize this discussion, Figure 8 shows a graphical comparison between the LQR and backstepping controllers, taking into account three key parameters:

- Robustness - measures the controller's ability to reject exogenous disturbances, measurement noise & model uncertainty;
- Performance - measures the controller's ability to follow the desired trajectory;
- (Easiness of) Tuning - measures the effort to tune the controller and adaptability to other launchers.

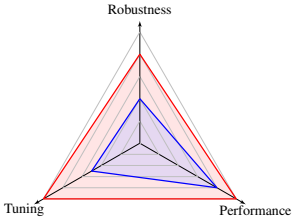

Fig. 8: Comparison of the LQR controller (blue), with the backstepping controller (red)

In terms of tuning, the backstepping controller is superior, as it only involves setting two matrix gains K_{ang} and K_w, while for the LQR controller it is necessary to tune the control effort and performance weight filters, in addition to solving the Riccati equation to obtain the controller gains. Furthermore, the adaptability of the LQR to other LVs is not straightforward. Regarding performance in the nominal condition, the LQR behaves similarly to the backstepping controller, albeit performance degrades for demanding trajectories.

As for robustness, it was seen that the backstepping controller is able to reject disturbances more satisfactorily, when compared to the LQR controller. Nevertheless, like in all other optimization processes, there is a trade-off between adaptability to other systems and mathematical complexity of the proposed control solution.

VI. Conclusion

Choosing a nonlinear control technique over linear control or vice-versa is not a trivial choice and several parameters influence this decision. Regarding adaptability to other LVs, nonlinear control has clear advantages since there are far less variables to consider than for linear control and Lyapunov analysis can be easily extended if the parameters of the system change. Major changes on the parameters of the system imply that the linearized models for which the linear controllers are developed are no longer valid and it is difficult to develop analytical guarantees for the stability of gain-scheduling techniques. On the other hand, linear control design is simpler that its nonlinear counterpart, as Lyapunov analysis can be quite cumbersome.

References

[1] Serdata, "World launcher review 2015-16," Commercial Space Technologies Limited, Serdata Limited, Tech. Rep., 2015.

[2] D. Dumitriu, P. U. Lima, and B. Udrea, "Optimal trajectory planning of formation flying spacecraft," *IFAC Proceedings Volumes*, vol. 38, no. 1, pp. 313–318, 2005.

[3] B. Wie, W. Du, M. Whorton, N. Marshall, and S. Flight, "Analysis and Design of Launch Vehicle Flight Control Systems," no. 515, pp. 1–11, 2008.

[4] J.-w. Jang, A. Alaniz, R. Hall, N. Bedrossian, C. Hall, and M. Jackson, "Design of Launch Vehicle Flight Control Systems Using Ascent Vehicle Stability Analysis Tool," in *AIAA Guidance, Navigation, and Control Conference*, 2011, pp. 1–16.

[5] J. S. Orr, J. H. Wall, and C. E. Hall, "Space Launch System Ascent Flight Control Design," in *2014 American Astronautical Society (AAS) Guidance, Navigation, and Control Conference*, 2014.

[6] E. N. Johnson and A. J. Calise, "Limited Authority Adaptive Flight Control for Reusable Launch Vehicles," *Journal of Guidance, Control, and Dynamics*, vol. 26, no. 6, 2003.

[7] A. Ngo and D. Doman, "Dynamic inversion-based adaptive/reconfigurable control of the X-33 on ascent," *Journal of Guidance, Control, and Dynamics*, vol. 25, no. 2, pp. 275–284, 2002.

[8] Arianespace, *Vega User's Manual*, 2014. [Online]. Available: http://www.arianespace.com/wp-content/uploads/2015/09/Vega-Users-Manual_Issue-04_April-2014.pdf

[9] C. R. Roux and I. Cruciani, "Roll coupling effects on the stability margins for vega launcher," *AIAA Structures, Structural Dynamics, and Materials Conference*, pp. 1–18, 2007.

[10] A. Marcos, V. Mantini, C. Roux, S. Bennani, and M. Carlo, "Bridging the gap between linear and nonlinear worst-case analysis : an application case to the atmospheric phase of the VEGA launcher," *19th IFAC Symposium on Automatic Control in Aerospace*, 2013.

[11] "Vega launcher characteristics," Available at https://blackboard.tudelft.nl/bbcswebdav/users/bzandbergen/LVC/Launch%20Vehicle%20Catalogue/Fiches/VEGA.pdf (11/08/2016), TU Delft, Tech. Rep.

[12] A. Marcon, L. Mangiacasale, and P. D. Resta, "Simulation model for VEGA control system design," *European Space Agency, (Special Publication)*, no. 606, pp. 137–142, 2006.

[13] A. Marcos, P. Rosa, C. Roux, M. Bartolini, and S. Bennani, "An overview of the RFCS project V&V framework: optimization-based and linear tools for worst-case search," *CEAS Space Journal*, vol. 7, no. 2, pp. 303–318, 2015.

[14] G. Baldesi and M. Toso, "ESA Launcher Flight Dynamics Simulator Used for System and Subsystem Level Analyses," *Advances in Aerospace Guidance, Navigation and Control: Selected Papers*, no. 1, pp. 434–437, 2011.

[15] C. Roux, V. Mantini, A. Marcos, L. F. Peñín, and S. Bennani, "Robust flight control system design verification & validation for launchers," *AIAA Guidance, Navigation, and Control Conference 2012*, pp. 1–9, 2012.

[16] F. Amato, E. Filippone, R. Iervolino, C. Italiano, and R. Aerospaziali, "Modelling and Guidance of a Small Conventional Launcher: The translational motion."

[17] J. Mulder, W. van Staveren, J. van der Vaart, and E. Al, *"Flight Dynamics"*, 2013.

[18] J. Diebel, "Representing attitude: Euler angles, unit quaternions, and rotation vectors," Stanford University, Tech. Rep., 2006.

[19] R. M. Murray, L. Zexiang, and S. S. Sastry, *"A Mathematical Introduction to Robotic Manipulation"*, 1994.

[20] M. S. Whorton, C. E. Hall, and S. A. Cook, "Ascent Flight Control and Structural Interaction for the Ares-I Crew Launch Vehicle," *AIAA Structures, Structural Dynamics, and Materials Conference*, pp. 1–13, 2007.

[21] E. Mooij, "The motion of a vehicle in a planetary atmosphere," 1994.

[22] B. Wie, *"Space vehicle dynamics and control"*. American Institute of Aeronautics and Astronautics, 1998.

[23] S. Bennani, A. Marcos, X. Lefort, and P. Simplício, "Structured Singular Value Analysis of the VEGA Launcher in Atmospheric Flight," *Journal of Guidance, Control, and Dynamics*, vol. 39, no. 6, pp. 1342–1355, 2016.

[24] T. Pulecchi, A. Marcos, C. Roux, V. Mantini, and S. Bennani, "Thrust Vector Control Robustness of axial-symmetric Launch Vehicles with Fuel Slosh," *AIAA Guidance, Navigation, and Control Conference*, pp. 1–10, 2012.

[25] N. Paulino, G. Cuciniello, I. Cruciani, F. Corraro, D. Spallotta, and F. Nebula, "Vega Roll And Attitude Control System Algorithms Trade-off study," *Progress in Flight Dynamics, GNC, and Avionics*, vol. 6, pp. 209–228, 2013.